

## Hybrid biofabricated blood vessel for medical devices testing

Alberto Portone<sup>a</sup>, Francesco Ganzerli<sup>a</sup>, Tiziana Petrachi<sup>a</sup>, Elisa Resca<sup>a</sup>, Valentina Bergamini<sup>a,b</sup>, Luca Accorsi<sup>a</sup>, Alberto Ferrari<sup>a,c</sup>, Simona Sbardelatti<sup>a</sup>, Luigi Rovati<sup>c</sup>, Giorgio Mari<sup>a</sup>, Massimo Dominici<sup>a,d\*</sup> and Elena Veronesi<sup>a\*</sup>

<sup>a</sup>Technopole "Mario Veronesi", Mirandola, Modena, Italy;

<sup>b</sup>Clinical and Experimental Medicine PhD Program, University of Modena and Reggio Emilia, Modena, Italy;

<sup>c</sup>Department of Engineering "Enzo Ferrari", University of Modena and Reggio Emilia, Modena, Italy;

<sup>d</sup>Department of Medical and Surgical Sciences, University Hospital of Modena and Reggio Emilia, Modena, Italy

### ABSTRACT

Current *in vitro* and *in vivo* tests applied to assess the safety of medical devices retain several limitations, such as an incomplete ability to faithfully recapitulate human features, and to predict the response of human tissues together with non-trivial ethical aspects. We here challenged a new hybrid biofabrication technique that combines bioprinting and Fast Diffusion-induced Gelation strategy to generate a vessel-like structure with the attempt to spatially organize fibroblasts, smooth-muscle cells, and endothelial cells. The introduction of Fast Diffusion-induced Gelation minimizes the endothelial cell mortality during biofabrication and produce a thin endothelial layer with tunable thickness. Cell viability, Von Willebrand factor, and CD31 expression were evaluated on biofabricated tissues, showing how bioprinting and Fast Diffusion-induced Gelation can replicate human vessels architecture and complexity. We then applied biofabricated tissue to study the cytotoxicity of a carbothane catheter under static condition, and to better recapitulate the effect of blood flow, a novel bioreactor named CuBiBox (Customized Biological Box) was developed and introduced in a dynamic modality. Collectively, we propose a novel bioprinted platform for human *in vitro* biocompatibility testing, predicting the impact of medical devices and their materials on vascular systems, reducing animal experimentation and, ultimately, accelerating time to market.

### ARTICLE HISTORY

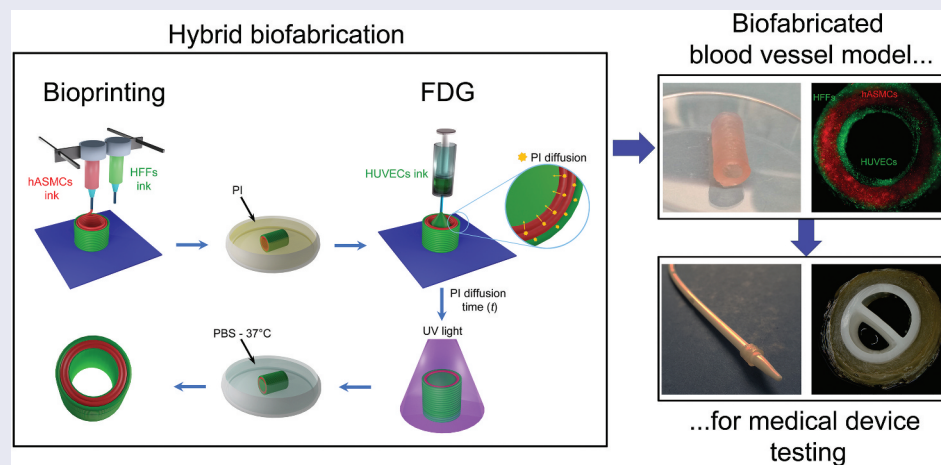
Received 15 July 2024

Revised 30 August 2024

Accepted 10 September 2024

### KEYWORDS

3D bioprinting; fast diffusion-induced gelation; three-layered artificial blood vessel; *in vitro* models; cytotoxicity assay; biocompatibility; medical device



### IMPACT STATEMENT

Our study provides an innovative convergence of 3D biofabrication technologies to realize multi-cellularized vessel-like models, as a new tool for *in vitro* biocompatibility testing of medical devices, minimizing animal experimentation.


## 1. Introduction

Currently, *in vitro* tests and animal models represent common methods to predict human response after contact with medical devices, as demanded by regulatory agencies [1,2]. Biocompatibility assessment is

mandatory for all medical device manufacturers [1]. Unfortunately, *in vitro* experimentation, which strictly relies on two-dimensional cultures, is strongly limited in terms of replicating the complex morphology, cellular organization, mechanical properties, and cell

**CONTACT** Elena Veronesi  [elena.veronesi@tpm.bio](mailto:elena.veronesi@tpm.bio)  Technopole "Mario Veronesi", Via 29 Maggio N 6, Mirandola 41037, Italy

\*Equally contributing authors.

 Supplemental data for this article can be accessed online at <https://doi.org/10.1080/14686996.2024.2404382>

© 2024 The Author(s). Published by National Institute for Materials Science in partnership with Taylor & Francis Group.

This is an Open Access article distributed under the terms of the Creative Commons Attribution-NonCommercial License (<http://creativecommons.org/licenses/by-nc/4.0/>), which permits unrestricted non-commercial use, distribution, and reproduction in any medium, provided the original work is properly cited. The terms on which this article has been published allow the posting of the Accepted Manuscript in a repository by the author(s) or with their consent.

interactions that typically occur in human tissues. In addition, although animal models can provide a higher level of biological complexity, they could not overcome interspecies variability and ethical concerns [3–5]. Models that could bypass the limitations of monocultures and animal experimentation might be three-dimensional (3D) system. These models are capable of including multiple cell types within the same structure, enabling the production of extracellular matrix and biomimicking cellular complexity in a simple and cost-effective manner [6]. Among the various areas of application, the need for a predictive model is particularly urgent in the study of cardiovascular diseases, the leading cause of death globally [7].

In this framework, considerable efforts have been dedicated to the realization of artificial blood vessels for various applications, such as vascular substitutes for grafts that bypass or replace occluded or damaged vessels [8] and *in vitro* models to study the pathogenesis of cardiovascular diseases [9]. A variety of techniques for the realisation of artificial blood vessels are known and well described, including microfluidic techniques [10], decellularization [11], annular mode casting [12], and additive manufacturing (AM) [8,13,14]. A new frontier of AM is bioprinting, an advanced technology able to offer an ethical and reliable alternative tool for toxicological evaluation, thanks to the ability to create 3D *in vitro* models that are inspired by the architecture of human tissues and organs, recapitulating their physiological complexity in an artificial living structure [15,16]. They retain a very relevant potential to enhance drug screening, *in vitro* studies, and high-throughput screening, while keeping in line with the 3Rs principle of replacement, reduction, and refinement of animal experimentation [17–20].

Among these, different families of 3D printing and bioprinting techniques, including extrusion [8,21,22], inkjet [23,24], stereolithography [25], two-photon [26], and co-axial printing [27], have been utilized with significant success due to their high geometric flexibility. Among them, extrusion-based bioprinting is the most widely applied approach due to the diverse range of hydrogels and biomaterials available nowadays [28]. However, its low resolution (approximately 200  $\mu\text{m}$ ) [29] limits the generation of thin cell layers, such as a typical endothelium of few tens of microns.

Recently, a diffusion-driven additive approach, called Fast Diffusion-induced Gelation (FDG), has been proposed [30–32] as a way to realize thin layered tubular structures. This method takes advantage of the rapid diffusion of ions or small molecules, such as photoinitiators (PIs) or enzymes, through gel–sol or gel–gel interfaces to produce hydrogel layers. Essentially, sacrificial cylindrical templates are impregnated with a crosslinking agent, and then immersed in a solution of hydrogel

precursors. As the crosslinker diffuses out from the template, it triggers the gelation of a layer of controlled thickness around the template. This approach has been successfully applied to the realization of concentric hollow structures made from various materials, including gelatin methacryloyl (GelMA) [31], alginate [31,32], and hydrogels obtained by free radical polymerization [33] or enzymatic cross-linking [30]. Moreover, the FDG offers the advantage to control the thickness of the layer by tuning the concentration of crosslinking agent and the diffusion time.

Here, we have challenged a new hybrid biofabrication approach that merges 3D bioprinting and FDG strategies to produce multi-cellularized vessel-like models that comprises three concentric layers of fibroblasts, smooth-muscle cells, and endothelial cells arranged from the outside in.

The bio-constructed model has been applied to assess the cytotoxicity of blood-contacting medical devices. We developed optimized protocols to replicate the device biological interaction that may occur in the patients, demonstrating the possibility to study the *direct contact* cytotoxicity of a commercial carbothane catheter by placing it inside the artificial vessel. To enhance the biomimicry of our biofabricated blood vessel (BBV), we additionally developed a miniaturized bioreactor named CuBiBox (Customized Biological Box) that allows vessel perfusion, enabling the future use of this artificial vessel in hemocompatibility studies or as a 3D model of circulatory system dysfunctions.

## 2. Materials and methods

### 2.1. 2D cell culture

Primary human foreskin fibroblasts (HFFs; American Type Culture Collection ATCC, Manassas, VE, U.S. A.) were seeded at a density of 8000 cells/cm<sup>2</sup> in Dulbecco's modified Eagle's medium (DMEM, Gibco, Waltham, MA, U.S.A.) containing 15% fetal bovine serum (FBS, Euroclone, Pero, IT), 1% penicillin/streptomycin (Gibco) and 2% glutamine (Gibco).

Primary human aortic smooth muscle cells (hASMC; ATCC) were seeded at a density of 5000 cells/cm<sup>2</sup> and cultured in a medium composed of vascular cell basal medium (ATCC) supplemented with a kit (ATCC) composed of recombinant human (rh) fibroblast growth factor-basic (final concentration of 5 ng/mL), rh insulin (5  $\mu\text{g/mL}$ ), ascorbic acid (50  $\mu\text{g/mL}$ ), L-glutamine (10 mM), rh epidermal growth factor (5 ng/mL), and 5% FBS.

Human umbilical vein endothelial cells (HUVECs; Lonza, Basilea, CH) were seeded at a density of 10,000 cell/cm<sup>2</sup> in endothelial growth medium-2 (EGM, Lonza) composed of endothelial basal medium-2

(EBM-2) and EGM-2 SingleQuots supplements (hydrocortisone, ascorbic acid, rh- epidermal growth factor, gentamicin sulfate amphotericin, insulin like growth factor, vascular endothelial growth factor, rh fibroblast growth factor-basic, heparin, and 2% FBS).

When confluence was reached, cells were detached with 0.05%/0.02% trypsin/EDTA (Gibco) at 37°C/5% CO<sub>2</sub>. Viable cells were counted with trypan blue 0.4% stain (Sigma, St Louis, MO, U.S.A.) and seeded at an adequate density in a flask or dispersed in the bioink for bioprinting process.

L929 murine fibroblasts (Sigma-Aldrich) were employed in cytotoxicity test to evaluate the CuBiBox bioreactor biocompatibility following the indications of the International Organization for Standardization (ISO10993-5:2009) [34]. Cells were seeded into 96-well plates (10,000 cells in 100 µL per well) and cultured for 24 h in a specific medium composed of DMEM (Gibco), 10% FBS (Euroclone), 2% glutamine (Gibco), and 1% Penicillin/Streptomycin (Gibco) at 37°C/5% CO<sub>2</sub>, and then the cells were employed in the cytotoxicity test as described below.

**2.2. Bioprinting process and fast diffusion-induced gelation**

3D Bioprinting was performed by using a commercial 3D printer (3D Bioplotter®, EnvisionTEC, Gladbeck, DE) under sterile flow hood cabinet. As schematized in Figure 1a, the cylindrical structure of the vessel was realized employing, in the same printing session, two bioinks loaded in two low-temperature printing heads set to 22°C. Except for the cellular component, both bioinks had the same formulation and were composed of (i) 6% w/v GelMA dissolved in DMEM (Sigma Aldrich) sterilized by 0.45 µm filtration, (ii) 0.32% w/v hyaluronic acid Sinovial HL 32 (IBSA, Massagno,

CH), and (iii) 0.5 mg/mL of the PI lithium phenyl-2,4,6-trimethylbenzoylphosphinate (LAP; Sigma Aldrich). The inks were loaded in a 30 ml plastic cartridge (Nordson, Westlake, OH, U.S.A.) compatible with the 3D printer and equipped with a plastic cap and a cylindrical metallic needle (Nordson) with an internal diameter of 250 µm. HFFs and hASMCs were dispersed into the first (HFFs ink) and the second ink (hASMCs ink), respectively, both cell types at the concentration of 2.5 × 10<sup>6</sup> cells/mL.

A customized computer-aided design (CAD) was created to realize the form of a cylinder composed of three concentric circles, for a final thickness of the vessel wall of about 1.5 mm. HFFs ink was used to produce the external circle, whereas the central and the internal circles were realized depositing hASMCs ink. The cylinder was built vertically, placed on one of the two bases. In this configuration, the printer realized the object extruding three concentric circles of material for each layer, using pneumatic pressure of 1 bar and printing speed of 5 mm/s. The process was conducted in a plastic plate placed on the printing platform cooled at 4°C. UV light (UV lamp, Thorlabs, Newton, NJ, U.S.A.; 170 mW/cm<sup>2</sup>) was provided for 5 s to the hydrogel every four printed layers to induce the crosslinking, stabilizing the structure, increasing the stability, and avoiding deformations or collapses. The realized cylindrical structures had about 1.5 mm width wall, 4 mm internal diameter, and up to 20 mm of maximum length (Figure 1b,c). After printing, scaffolds were cultured in HFFs and hASMCs medium in a 1:1 ratio and incubated at 37°C, 5% CO<sub>2</sub> to provide adequate cell culture conditions.

After 24 h, the endothelial layer was added to the structure by FDG (Figure 1a). The hydrogel for FDG (HUVECs ink) was realized using the same preparation protocol described for bioprinting inks but

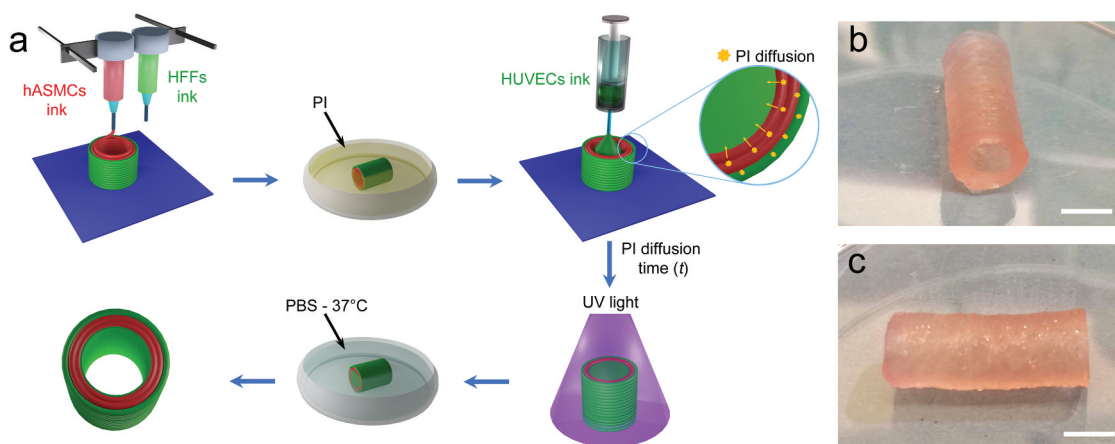


**Figure 1.** (a) Schematic representation of the hybrid biofabrication process. Cylinder structure composed of three concentric, circular layers is bioprinted using an extrusion 3D printer. The external layer in green is printed with HFF ink, and the two internal layers in red are printed with hASMCs ink. Then, the cellularized cylinder is soaked with a solution of PI for 30 min. Later, the cylinder is placed vertically and is filled with HUVECs ink. After a specific PI diffusion time (t), the structure is irradiated with UV light and is placed in PBS at 37°C to remove the non-crosslinked ink, finally obtaining a hollow and layered cylinder. (b,c) Photographs of the artificial vessel from different sides. Scale bar = 5 mm.

without PI and adding HUVECs cells at a density of  $10 \times 10^6$  cells/mL. The HUVECs ink was loaded in a 5 mL syringe and stored at 23°C until use. Bioprinted cylinders were soaked with LAP PI solutions at different concentrations (0.4, 0.5, 0.6, 0.8, and 1 mg/mL in PBS). Then, cylinders were placed vertically in the middle of a plastic Petri and filled with the HUVECs ink. After a selected diffusion time (15 or 30 s), the cylinders were irradiated with UV light using a UV lamp ( $\sim 90$  mW/cm<sup>2</sup>) for 10 s. Immediately after irradiation, the cylinders were immersed in PBS and kept at 37°C with stirring for 30 min and then placed in culture medium in an incubator at 37°C and 5% CO<sub>2</sub>.

For three-layer artificial vessel culture, a medium composed of HUVECs and hASMCs media in a ratio of 1:1 was employed.

### 2.3. Histology and immunofluorescence

Histological analysis was performed after 5 days of culture, fixing the BBV in 2.5% v/v glutaraldehyde solution (Sigma-Aldrich) in PBS for 24 h. After dehydration in ascending series of alcohols (Histo-Line Laboratories, Milan, IT), samples were embedded in paraffin, cut in 4 μm slices by microtome (Leica RM2255, Leica, Wetzlar, DE), and collected on glass slides.

For hematoxylin and eosin (H&E) staining, the section was deparaffinized in HistoClear (Histo-Line Laboratories, Milan, IT) and rehydrated in descending alcohols. After rinsing in distilled water, the slices were stained in Carazzi's hematoxylin solution (Histo-Line Laboratories) and in eosin Y solution (Carlo Erba reagents, Cornaredo, IT), dehydrated, mounted using DPX Mountant (Sigma Aldrich), and observed by optical microscope Axio Imager M2 (Zeiss, Oberkochen, DE) at 200× of magnification. Images were then acquired by ZenPro Software (Zeiss).

BBV specimens, deparaffinized as previously described, were also stained by indirect immunofluorescence assay. Samples were retrieved in citrate buffer (pH 6) for 15 min at 96°C and 20 min at room temperature and incubated for 30 min with a blocking solution composed by maleic acid (Sigma Aldrich), blocking reagent (Roche, Basilea, CH), and newborn calf serum (Euroclone) in a 3:1:1 volumetric ratio. Then, samples were incubated with the primary antibody rabbit anti-human CD31 (Abcam, Cambridge, UK, ab28364; 1:50) and rabbit anti-human von Willebrand Factor (anti-vWF, Abcam, ab6994; 1:300) primary antibodies produced in rabbit, for 1 h at room temperature. After three washes in PBS, samples were incubated for 1 h at room temperature with red fluorescent anti-rabbit secondary antibody (Invitrogen, Thermo Fisher Scientific, Waltham, MA, U.S.A.; 1:500). Nuclei were counterstained with DAPI (Thermo Fisher Scientific) for 5 min at room

temperature. Stained samples were observed by AxioZoom V16 (Zeiss) and by AxioImager M2 (Zeiss) optical microscopes at 270× and 400× of magnification. Images were acquired by ZenPro Software (Zeiss).

### 2.4. Cell viability assays and vital cell tracking

Live & dead staining was performed by using the LIVE/DEAD™ cell viability/cytotoxicity assay kit (Thermo Fisher Scientific). Briefly, samples were stained with 1 mL of the live & dead solution, containing calcein and ethidium bromide, prepared following manufacturer's instructions, and incubated for 45 min at 37°C and 5% CO<sub>2</sub>. Then, the samples were rinsed in PBS and immediately observed by AxioZoom V16 (Zeiss) at 100× and 270× of magnification.

To identify the cell types within the BBV, HFFs, hASMCs, and HUVECs were labelled before bioprinting using two different vital cell trackers. HFFs and HUVECs were marked with a green fluorescent tracker (CellTracker™ Green CMFDA, Invitrogen), while hASMCs were marked with a red fluorescent tracker (Qtracker™ 605 Cell Labeling Kit, Invitrogen) following manufacturer's instructions.

Fluorescence imaging was performed using the Axio Zoom V16 microscope (Zeiss) at 15×, 40×, and 60× of magnification.

To evaluate the correlation between the PI concentration, the diffusion time and the HUVEC layer thickness, HUVEC cells incorporated in the BBVs were labelled with green fluorescent vital tracker to highlight the layer obtained by FDG. Images were acquired using the Evos FL microscope at 4× of magnification. The thickness of the layer was measured by the image analysis software ImageJ.

Cell viability was also assessed by 3-(4,5-dimethylthiazol-2-yl)-2,5-difeniltetrazolio (MTT) assays after 24 h of exposure to the eluates of tested materials, obtained by dipping them in an adequate volume (1 mL per 0.2 g of material as reported by ISO 10993,12) [35] of culture medium for 24 h. Then, cultures were incubated with 1 ml of MTT solution (Sigma-Aldrich, 1 mg/mL in DMEM) for 2 h at 37°C. Then, the MTT solution was removed, and the MTT salts were solubilized in 1 mL of isopropanol (Sigma-Aldrich) per sample. The detection of cell viability was performed by quantifying the optical density at 570 nm of the MTT salts solubilized in isopropanol, using a multiplate reader spectrophotometer (Enspire, PerkinElmer, Hopkinton MA, U.S.A.). The reduction in cell viability compared with a control sample not exposed to the eluates was determined using the following formula:

$$\text{Cell viability(\%)} = \frac{OD_{570e}}{OD_{570b}} \times 100$$

where  $OD_{570e}$  is the mean value of the measured optical density of the eluate, and  $OD_{570b}$  is the mean value of the measured optical density of the control sample at 570 nm wavelength. A material is considered non-cytotoxic by the international standard ISO10093-5:2009 if the cell viability is higher than 70% compared to a control sample not exposed to the extract [34].

## 2.5. Cytotoxicity tests on BBV

The impact on BBV of a commercially available carbothane catheter (OMNlath®, B.Braun Avitum, Mirandola, IT) was evaluated by co-culture accounting both *indirect* and *direct contacts*.

*Indirect contact* cytotoxicity was tested by live & dead and MTT assays, performed on BBV cultured for 24 h with the eluates of the mentioned commercial catheter. The high-density polyethylene (HDPE, Sigma-Aldrich), a polymer known to be biocompatible, and the sodium dodecyl sulphate (SDS, Adventa Health, Kota Bharu, MY), known to be strongly cytotoxic if used at the concentration of 0.1% w/v, were employed as negative and positive controls, respectively, according to ISO10993-12:2021 and ISO10993-5:2009 [34,35]. The tests were conducted in triplicate, and the viability of three BBV, cultured without any eluate (CTRL), was used to normalize all the other samples.

MTT assay was performed as previously described, after 24 h of BBV exposure to the eluates.

The viability of BBV samples exposed to eluates was also assessed using a live & dead assay, following the previously described protocol. For the evaluation of *direct contact* cytotoxicity, the catheter was introduced into the BBV and was co-cultured for 24 h. The BBV cell viability was determined by a live & dead assay. Subsequently, the BBV with the catheter inside was carefully cut and imaged, acquiring both bright field and fluorescent microscopy (Axio Zoom V16, Zeiss) focusing on cell viability in contact with the catheter. The test was conducted in triplicate.

## 2.6. Miniaturized bioreactor for vessel perfusion

To perfuse the BBV, a bioreactor defined as CuBiBox has been designed and realized. CuBiBox is composed of (i) a screwable lid in polytetrafluoroethylene (PTFE) with a gas permeable membrane in polymethylpentene for gas exchange, (ii) a cylindrical culture chamber in PTFE with a central groove that host the vessel, and (iii) four luer lock connectors (two with a conical tip and two with a flat tip) in polyether ether ketone (PEEK) to perfuse the vessel connecting it to a peristaltic pump (connectors with conical tip), and to change the medium inside the chamber (connectors with flat tip). The device has been designed by Solid

Works® (Standard, 2019) and the components have been made in a mechanical workshop (Goldoni e Dondi srl, Medolla (MO), Italy), obtaining the desired structures by precision machining and machine tools for swarf removal.

The lid geometry and the use of the gas exchange membrane were inspired by a bioreactor previously developed by our group [36], and it ensured the isolation of the culture chamber from external contaminants and pathogens. Finally, it was sterilized in an autoclave at 121°C at a pressure of 5 bar for 20 min before use.

Bioreactor biocompatibility was assessed by MTT cytotoxicity tests according to International Organization for Standardization (ISO10993-5:2009) [34] that defines the standardized procedures to evaluate the cytotoxicity of a material or a medical device. As required by regulation, L929 murine fibroblasts (Sigma-Aldrich) seeded into 96-well plates were stimulated with the eluate obtained from the bioreactor. Eluate was prepared filling the culture chamber with DMEM (Gibco) containing 10% FBS (Euroclone) and 1% Penicillin/Streptomycin (Gibco) for 24 h at 37°C and stirring. Then, the eluate was sterilized by filtration with a 0.2 µm filter. Latex and HDPE extracts were introduced, respectively, as positive and negative controls [32], and after 24 h of stimulation, cell viability was evaluated by MTT assay as previously described.

The performances of the bioreactor were evaluated culturing an artificial vessel in perfusion (30 mL/min) for 24 h, connecting the bioreactor to a peristaltic pump (Gilson, Middleton, WI, U.S.A.; minipuls® 3). Cell viability was characterized by live & dead assay using the Axio Zoom V16 microscope (Zeiss).

## 2.7. Statistical analysis

Data are expressed as means ± standard deviation. For MTT cytotoxicity assays, results were analyzed by Student's t-test, and p-values were obtained to compare the means between samples treated with eluates and the untreated control.  $p$  value < 0.05 (\*), < 0.01 (\*\*), and < 0.001 (\*\*\*) were considered statistically significant.

## 3. Results

### 3.1. Fast diffusion-induced gelation as performing strategy for HUVEC layer biofabrication

We began our study by an extrusion 3D printing approach [28], where bioprinting parameters were investigated for the realization of a cylindrical structure. In the first phase, we tested the impact of the printing process on cell viability for HFFs, hASMCs,

or HUVECs after 24 h, using live & dead assay. For all the cell types, bioprinting was conducted mixing the cells with a bioink composed of 6% w/v GelMA, 0.32% w/v HA, and 0.5 mg/mL PI and extruding the material through a cylindrical needle with an internal diameter of 250  $\mu\text{m}$ .

Although we found a good viability for both HFFs and hASMCs (Figure S1 of Supplementary Material), HUVECs showed a high mortality (Figure 2a). Moreover, the extrusion 3D printing approach employed for the bioprinting resulted in significant limitations in resolution, which is nominally of about 200  $\mu\text{m}$  [29]. The most appropriate strategy to improve the resolution of the extrusion 3D printing process was the use of small diameter needles (<100  $\mu\text{m}$ ) that unfortunately affected cell viability due to the friction stress during extrusion.

To reduce the mortality of HUVECs during biofabrication and to obtain an endothelial layer as thin as possible to mimic the actual size of the vascular endothelium, we introduced the FDG procedure, allowing the deposition of a thin hydrogel layer populated by HUVECs on the walls of the vessel lumen, preserving the cell viability better than 3D extrusion bioprinting (Figure 2b). Indeed, after 24 h in culture, the percentage of dead HUVECs by extrusion 3D bioprinting was  $32.4 \pm 2.8\%$ , while with FDG, this level was significantly reduced to  $4.3 \pm 1.2\%$  (Figure 2c).

FDG offered the opportunity to control the thickness of the layer by tuning the PI concentration and the diffusion time, i.e. the time between HUVECs ink injection and UV light irradiation. Figure 3a,b shows the dependence of HUVECs layer thickness on the concentration of PI. We performed the FDG process using green fluorescent HUVECs labelled with a vital tracker, and we evaluated the thickness of the cellularized layer obtained with PI concentration between 0.4 and 1 mg/mL, and a fixed diffusion time of 30 s. PI

concentration of 0.6 mg/mL forms a layer with a thickness of <200  $\mu\text{m}$  ( $185 \pm 34 \mu\text{m}$ ), which is a smaller mean value than the minimum thickness obtainable with bioprinting [29]. Lowering the PI concentration further to 0.5 mg/mL produces a layer of  $154 \pm 28 \mu\text{m}$ , while concentrations equal or lower than 0.4 mg/mL do not produce a uniform layer or are not sufficient to ensure the adhesion of the endothelial layer to the bioprinted cylinder. Above 0.5 mg/mL, there is a linear correlation between the concentration of PI ([PI]) and the thickness of the inner layer ( $d$ ), which follows the formula  $d = S[\text{PI}]$  with a slope  $S$  of approximately 340  $\mu\text{m}/(\text{mg/mL})$ . As previously reported [37], this relationship depends on the diffusion of the cross-linking agent, and allows the thickness of the FDG-deposited layer to be precisely tuned by adjusting the PI concentration. Although PI concentrations lower than 0.5 mg/mL cannot be used, the thickness of the endothelial layer can be further reduced to  $85 \pm 23 \mu\text{m}$  by decreasing the diffusion time to 15 s, as shown in Figure 3c.

As reported in Figure 3d, the FDG biofabrication approach produces a uniform layer of endothelial cells for the entire length of the vessel. Indeed, when the endothelialized cylindrical structure is cut at four different points, the resulting thickness of the HUVEC-populated region remains quite uniform.

### 3.2. A hybrid biofabrication allows the correct cell stratification in the BBV

Having selected the FDG as the most performing approach to introduce HUVECs layer, we then generated a complete BBV with all the three cell types (HFFs, hASMCs, and HUVECs) arranged in concentric layers by hybrid biofabrication. This approach involved two key steps. First, we bioprinted a hollow cylinder utilizing two print heads simultaneously: one loaded with HFFs ink used to bioprint the outer layer

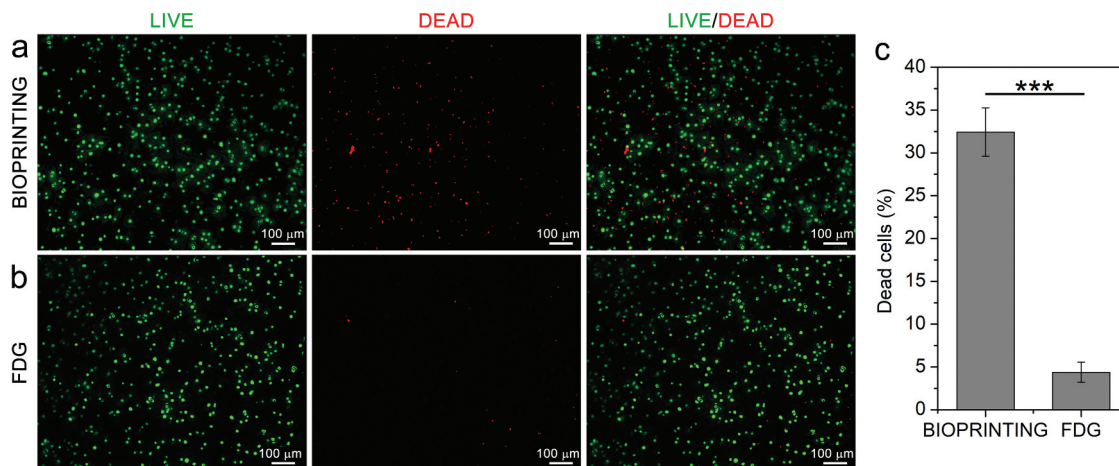


**Figure 2.** Live & dead assay of HUVECs. (a,b) Micrographs of HUVECs in GelMA matrix deposited by bioprinting (panel a) or FDG (panel b) after treatment with live & dead kit, which label in green the living cells and in red the dead cells. (c) Comparison of HUVECs mortality within a hydrogel structure fabricated via bioprinting versus FDG. Significance was set at  $p < 0.001$  (\*\*\*).

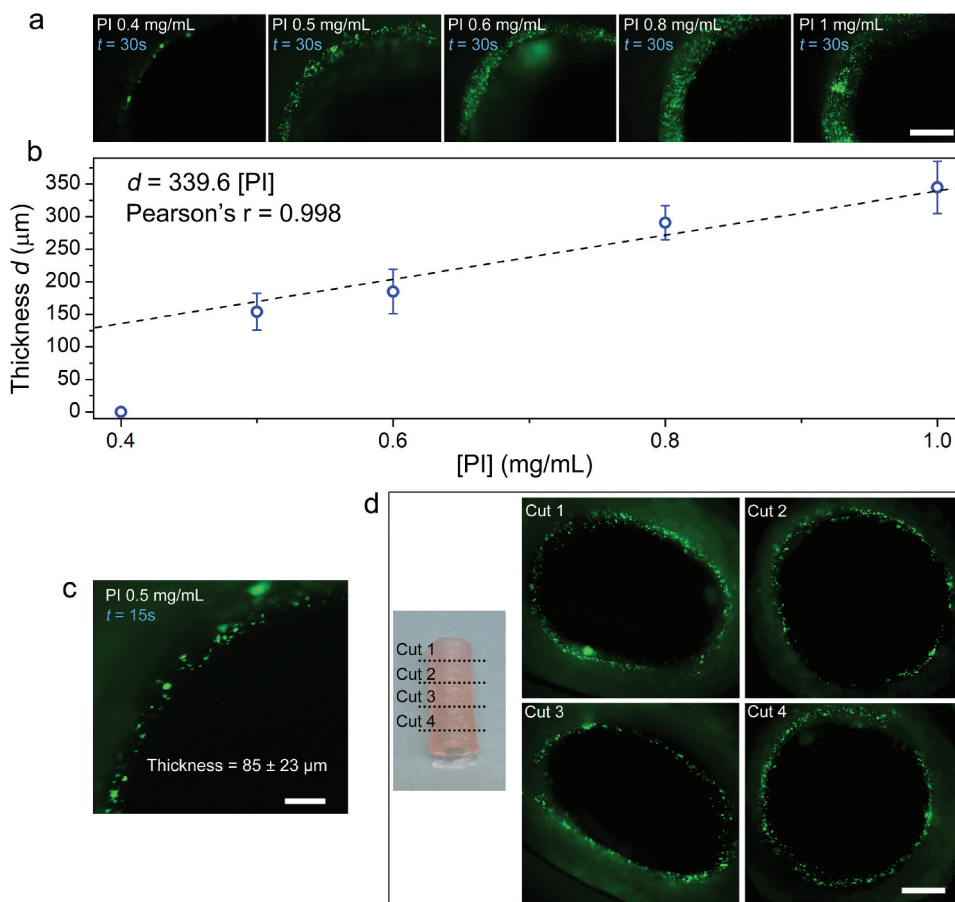


**Figure 3.** Characterization of the HUVECs layer obtained by FDG. (a) Micrographs of the endothelial layer populated by HUVECs (marked in green) realized by FDG using different concentrations of PI (from 0.4 mg/mL to 1 mg/mL) and a diffusion time ( $t$ ) of 30 s. Scale bar = 0.5 mm. (b) The graph correlates the thickness of the obtained layer vs the PI concentration; dashed line is a linear fitting of data set from 0.5 to 1.0 mg/mL PI. (c) Micrograph of the endothelial layer obtained with PI concentration of 0.5 mg/mL and diffusion time of 15 s. Scale bar = 0.1 mm. (d) Endothelial layers of an artificial vessel observed at different cutting points along the lines indicated in the photograph on the left (cut 1-4). Scale bar = 1 mm.

and the other with hASMCs ink to bioprint the intermediate layer. Second, we deposited the inner endothelial layer using the FDG technique. Figure 4a, b shows the section of two artificial vessels with the three concentric layers populated by HFFs (labelled in green), hASMCs (labelled in red), and HUVECs (labelled in green) from outside to inside. The method guarantees the separation and the appropriate cell localization, and, thanks to its versatility, it further gives the opportunity to control the thickness of the internal layer. Therefore, we produced two BBVs with different endothelial layer thickness. The thin endothelial layer (Figure 4a) was obtained using 0.5 mg/mL of PI and diffusion time of 15 s, while the thick layer (Figure 4b) was realized with 0.6 mg/mL of PI and diffusion time of 30 s. In the two types of BBV obtained, histological characterization was performed.

The H&E staining (Figure 4c,d) confirms the correct stratification of the three cell populations in the different layers. In addition, the staining highlights the porosity status of the endothelial layer, showing larger pores in comparison to the bioprinted bilayer. Immunofluorescence analysis demonstrates that,

after FDG, HUVECs preserve their phenotypical features, expressing the endothelial markers CD31 (Figure 4e,f) and vWF (Figure 4g,h). Immunofluorescence underlines the localization of HUVECs in the layer obtained by FDG. When the process is set to obtain a thin endothelium (Figure 4a,c,e,g), HUVECs organize themselves in a single-cell or few-cells layer. In a thicker endothelium (Figure 4b,d,f,h), HUVECs are able to migrate and self-organize along the outer and inner borders (see white arrows in Figure 4f,h), assembling themselves to form thin endothelial-like structures. For the further assays, we selected the BBV obtained with thin endothelial layer, which more closely resemble the architecture of a human blood vessel.

### 3.3. The BBV as novel model for cytotoxicity evaluation

To evaluate the potential of the BBV model to serve as a platform for biocompatibility testing of blood-contacting biomedical devices, we evaluated the cytotoxicity of a commercial catheter for blood circulation

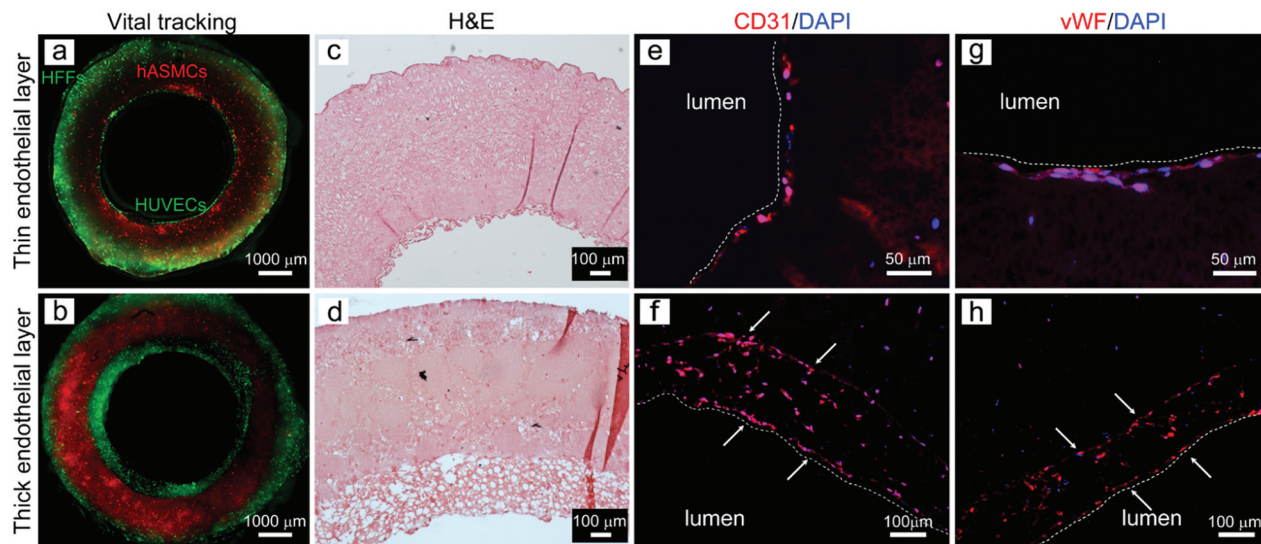


**Figure 4.** Characterization of BBVs. (a,b) Sections of two artificial vessels populated by HFFs (labelled in green), hASMCs (labelled in red) and HUVECs (labelled in green). The different thickness of the internal layer is due to a different FDG protocol employed in the fabrication: 0.6 mg/mL and diffusion time of 30 s in a, 0.5 mg/mL and diffusion time of 15 s in b. c,d) H&E labelling of slices of artificial vessels with thin (c) or thick (d) endothelial layer. e-h) Immunofluorescence staining of the BBV showing the expression of CD31 (c,d) and vWF (e,f) endothelial markers. White arrows indicate HUVECs cells self-organized along the outer and inner borders of the layer.

in two ways: *direct contact* (Figure 5a-c) and *indirect contact* (Figure 5d-h).

The catheter was inserted inside the BBV to obtain a *direct contact*. After co-culture of 24 h, the fluorescent staining obtained with live & dead assay showed only live (green) cells, also in the area of interaction with the catheter (see arrows in Figure 5c), suggesting no apparent cytotoxicity due to catheter contact and the feasibility of inserting the device inside the blood vessel without inducing cell death.

We then applied the BBV for *indirect contact* cytotoxicity studies, and we adapted the MTT protocol according to ISO10993-12:2021 [35] and ISO10993-5:2009 [34] and ISO10993-23:2021 [38]. Eluates obtained by catheter (CE), HDPE and SDS as negative and positive controls, respectively, were administrated to the BBVs. In parallel to MTT to confirm the possible cytotoxicity of medical device, live & dead assay was performed.

Both methods showed similar results confirming the non-cytotoxic profile of the analysed catheter, as reported in Figure 5d-h. The CE and HDPE did not impact on the viability of the cells in the vessel, which is of  $103.9 \pm 9.9\%$  and of  $104.3 \pm 5.6\%$ , respectively, compared to the untreated CTRL ( $100.0 \pm 3.7\%$ ;  $p$  value  $> 0.05$ ). On the contrary and as expected, SDS caused a strong mortality, showing a cell viability of  $23.6 \pm 1.1\%$  compared to the CTRL ( $p$  value  $< 0.001$ ) (Figure 5h). These findings were comparable with the ones obtained by live & dead assay (Figure 5d-g), where fluorescent imaging of the vessels shows a prevalence of green (live) cells in the CTRL, CE, and HDPE samples in all the BBV layers, while in SDS-

treated sample, the fluorescent red signal was strongly prevalent, indicating cell death in the entire construct.

Overall, these data demonstrate the possibility to employ the artificial vessel as innovative platform to assess the cytotoxicity of medical devices.

### 3.4. The BBV as core technology within a bioreactor in dynamic perfusion assays

Having generated a suitable BBV, we wanted to create a novel bioreactor conceived and realized with the purpose of connecting BBV to a peristaltic pump to allow a perfusion with a controlled flow. The bioreactor was called 'CuBiBox'. Figure 6a,b schematizes the components of the bioreactor. The vessel is placed in the central groove of the culture chamber, with the two conical connectors (A) that are inserted in its lumen (Figure 6b) blocking it. The flat connectors B are screwed to the culture chamber, perpendicularly respect to the connectors A. Connectors A directly link the inner structure of the vessel to a peristaltic pump, while connectors B allow to inject fresh medium inside the culture chamber without opening the box. The entire bioreactor has a diameter of 5 cm and a height of 2.5 cm (Figure 6c), and it is constituted by materials known to be biocompatible, as confirmed by the biocompatibility test performed accordingly to the ISO10993-5:2009 [34] (Figure 6d). Cytotoxicity assay was performed by using L929, a well-characterized fibroblastic cell line isolated from the murine connective tissue. This ISO recommend the use of L929 due to their reliability, sensitivity, and standardization,



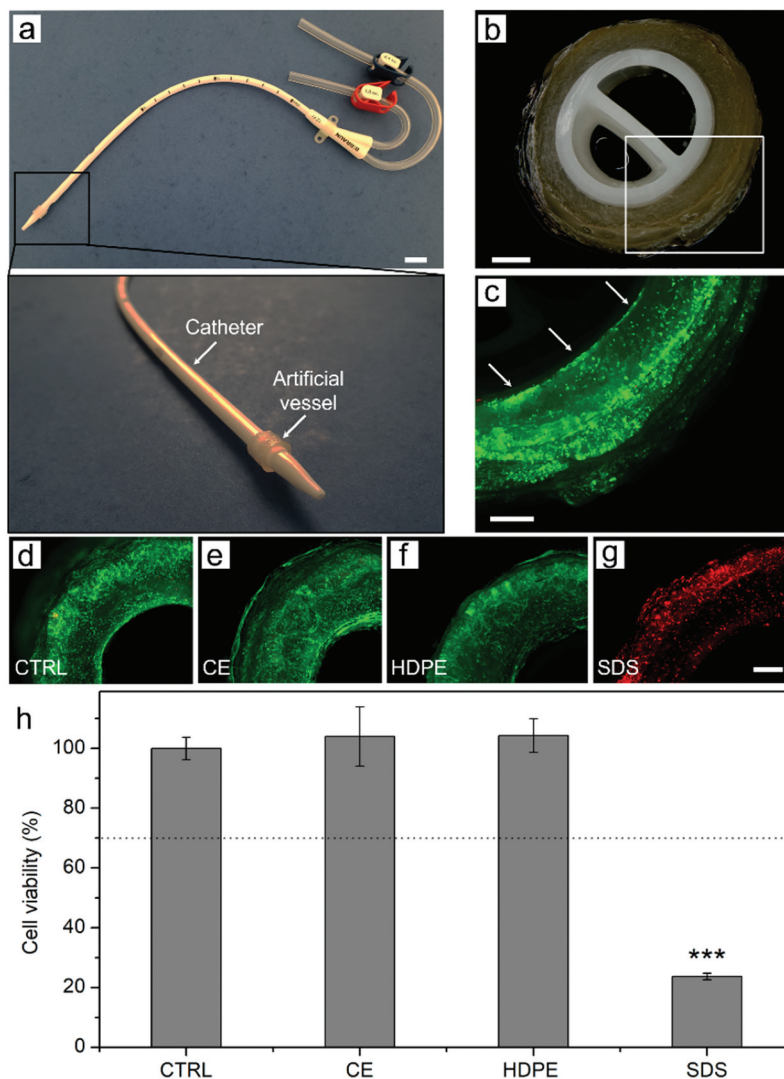


**Figure 5.** Cytotoxicity evaluation of a blood-contacting biomedical device. (a-c) Study of contact cytotoxicity of a catheter after 24 h of insertion in the vessel. The test was performed placing the medical device inside the artificial vessel (a). Scale bar = 10 mm. (b) Bright field micrograph of a section of the vessel with the catheter inside. Scale bar = 1 mm. (c) Viability evaluation performed by live & dead assay in the region indicated by the white rectangle in b. The arrows indicate the contact region between the vessel and the catheter. Scale bar = 0.5 mm. (d-g) Live & dead assay of artificial vessels cultured for 24 h in standard culture medium (CTRL, d), in the extract of the intravenous catheter (CE, e), in the extract of a biocompatible polymer (HDPE) as negative control (f), and with a solution of SDS as positive control (g). Scale bar = 0.5 mm. (h) Viability evaluation of the same samples assessed by MTT assay. Significance was set at  $p < 0.001$  (\*\*\*)

making them a valuable tool for assessing the safety of materials in contact with the human body.

The viability of L929 cell line exposed to the eluate of the CuBiBox was of  $89.2 \pm 11.0\%$ , comparable with negative control ( $90.7 \pm 7.5\%$ ) and statistically higher than positive control ( $5.1 \pm 0.7\%$ ;  $p$ -value  $< 0.001$ ). Being the viability of the cells cultured with the CuBiBox eluate higher than 70%, the bioreactor was considered as non-cytotoxic accordingly to ISO10993-5:2009 [34]. Figure 6e,f, respectively, reports BBVs cultured in static and dynamic conditions, and then labelled with live and dead assay. It shows no significant differences in terms of cell viability.

The same perfusion/static comparison was performed on two artificial vessels realized using fluorescent labeled HUVECs to highlight the structure

of the internal layer. The insets of Figure 6e,f demonstrate that the HUVEC-populated layer cultured in perfusion for 24 h (inset of Figure 6e) does not show damages or differences if compared with the vessel cultured in static conditions (inset of Figure 6f). The perfusion process showed no changes in the size of the BBV, having inner diameter of  $3970 \pm 117 \mu\text{m}$ , outer diameter of  $7256 \pm 58 \mu\text{m}$ , and wall thickness of  $1580 \pm 100 \mu\text{m}$ , comparable with the sample cultured in static conditions (inner diameter of  $3980 \pm 120 \mu\text{m}$ , outer diameter of  $7260 \pm 140 \mu\text{m}$  and wall thickness of  $1600 \pm 55 \mu\text{m}$ ). Thus, the bioreactor itself and the perfusion procedures do not alter the BBV cell viability, in particular the internal layer is not impacted by mechanical stress of the flow.

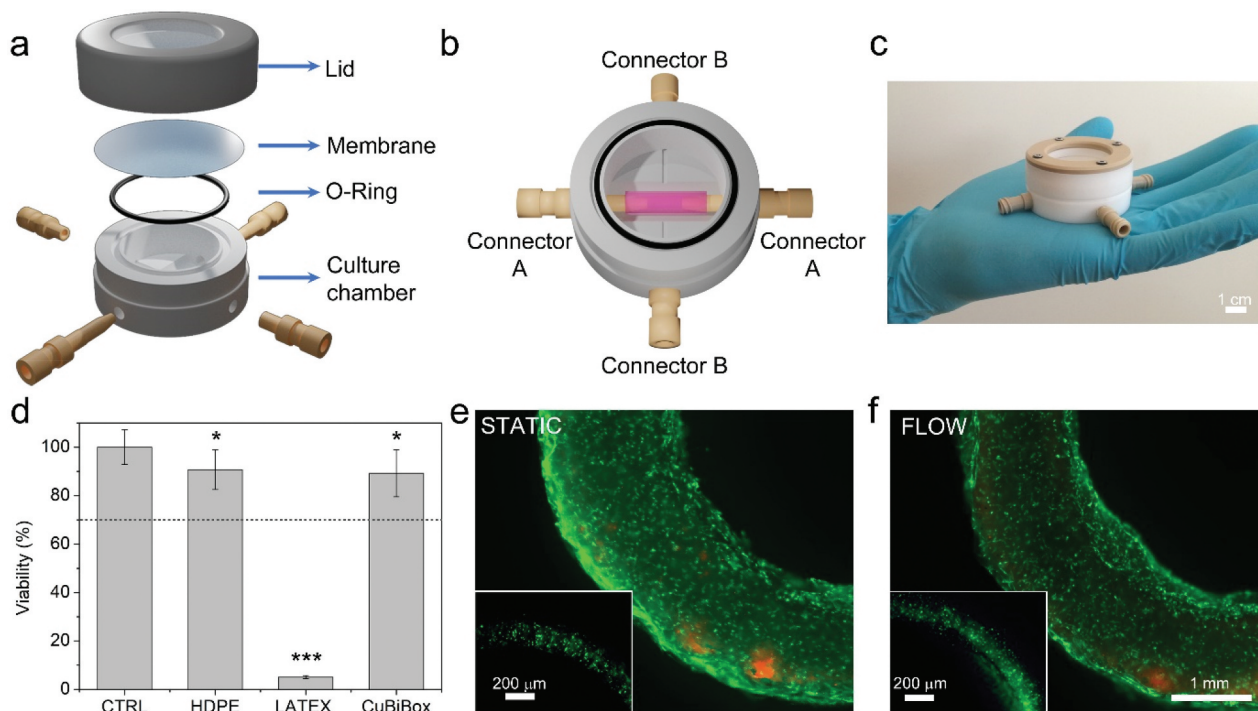


**Figure 6.** CuBiBox bioreactor characterization. (a,b) Schematic representation of the CuBiBox bioreactor showing its components (a) and the top view with the artificial vessel (in pink) placed in the central groove of the box (b). (c) Photograph of the assembled bioreactor. (d) MTT test performed on the CuBiBox extract to evaluate the cytotoxicity of the final device. Significance was set at  $p < 0.05$  (\*) and  $p < 0.001$  (\*\*\*). (e,f) Live & dead assay on the artificial vessel cultured for 24 h in static conditions (e) or in perfusion (f) inside the CuBiBox bioreactor. The insets show the internal layer populated by green labelled HUVECs cultured in static (e) or dynamic (f) conditions.

#### 4. Discussion

3D models offer several advantages over 2D cell culture and *in vivo* assay for toxicology investigations including an increase in biomimicry with human tissue, improved predictivity, cost-effectiveness, and high-throughput screening capabilities [36]. In this framework, biofabrication technologies represent a further innovation for *in vitro* models of human tissues and organs, whether in healthy [13,19,39] or pathological conditions [6,40]. Based on 3D co-culture of cells, which are precisely localized in a three-dimensional structure, these biofabricated products are demonstrating a very relevant biomimetic potential in accurately replicating the intricate architecture of human tissues.

In this study, we realized a three-layer BBV populated by fibroblasts, smooth muscle cells, and endothelial cells organized as in arteries and veins of human body, as *in vitro* model for biocompatibility assessment of biomedical devices. Unlike the cytotoxicity assay specified by the guidelines [34], requiring the use of only murine fibroblasts in monolayer, the 3D co-culture of the artificial vessel, given the ability to recapitulate the existence of three different cell types and the correct spatial organization, offers a more complex and a more biomimetic platform for prediction of the cytotoxic potential.

Multilayer vessel-like structures have been previously realized by using specialized and customized equipment, i.e. using coaxial needles or customized extruders [9] or with the help of sacrificial support materials [41]. The combined bioprinting and FDG strategy relies on the use of a readily available commercial extrusion 3D printer. In addition, avoiding the use of sacrificial materials, no additional steps need to be performed, limiting the possibility of contamination, and making this approach simple and versatile. To improve the printability and the stability of the cylindrical construct during biofabrication without adding sacrificial supports, we provided a specific UV dose every four layers. Also the introduction of hyaluronic acid to the ink formulation improved the printability [8] and, at the same time, provided functional stimuli to the cells embedded in the matrix. Indeed, it has been reported that hyaluronic acid increases spreading and proliferation of fibroblasts [42], and enhances cell-matrix adhesion of smooth muscle cells and endothelial cells, that strongly express hyaluronic acid receptors such as CD44 [43,44].

Recently, Xu and colleagues realized bioprinted self-standing artificial vessels populated by hASMCs and HUVECs in two distinct layers [8]. Although the described strategy provides a correct compartmentalization of the two cell types, the endothelial cell layer results at least 200 μm thick with endothelial cells indistinctly dispersed inside the matrix. Indeed, the

extrusion 3D printing approach employed for the bioprinting is strongly limited in resolution, which is nominally of about 200  $\mu\text{m}$  [29]. A possible strategy to improve resolution is the use of small diameter needles which, however, affects cell viability due to frictional stress during extrusion.

To overcome such resolution limitation, we employed FDG for the realization of the endothelial layer reducing its thickness up to  $\sim 80 \mu\text{m}$  and localizing HUVECs in a thin layer in which cells are close to each other and have the possibility to develop correct cell-cell interactions. Strikingly, when we increase the thickness of the endothelial layer with a longer FDG diffusion time, we observe that endothelial cells can migrate and, in just 4 days, self-organize in endothelial-like structures along the outer and inner edges. Such unexpected behavior, is probably due to the porosity of the matrix deposited by FDG. Indeed, HUVECs generally do not show migratory behaviors in bioprinted GelMa scaffolds as shown in previous works [8] and as well as observed in preliminary experiments (data not shown). The porous architecture probably allows HUVECs to move between pores, encountering low resistance to migration through the hydrogel meshes [45]. Noteworthy, in comparison to the extrusion process, FDG strategy minimizes the mechanical stress experienced by endothelial cells during the biofabrication, strongly reducing cell mortality.

The selected bioink formulation represents an optimal microenvironment for cell survival and proliferation. The chosen concentration of 6% w/v for the biofabrication process ensures excellent printability, which is a crucial parameter allowing the precise deposition of the concentric cylindrical structure. Xu L. et al. described the biofabrication of blood vessel-like grafts by using a bioink formulation (GelMA 6% w/v; gelatin 2% w/v; HA 0.3% w/v) similar to that described in our work. The authors analysed in detail the mechanical properties of the hydrogel, reporting a Young's modulus of approximately 35 kPa and a tensile stress of about 12 kPa [8]. Literature reports a large number of biofabrication papers based on the use of GelMA in the range concentrations of 4–10% w/v. In this range, mechanical properties of GelMA bioinks are well described and show a Young's modulus ranging from a few kPa to tens of kPa and tensile strength ranging between  $\sim 10$  kPa and  $\sim 100$  kPa [46–49]. It is therefore reasonable to assume that the Young's modulus and tensile strength of our biofabricated blood vessels fall within this range.

The three different types of human cells, typically found in blood vessels, organized in a biomimetic 3D configuration, suggest that BBV could be applied as predictive platform to evaluate the cytotoxic effect of intravascular medical devices. The three-dimensionality of the model allows to perform complex *in vitro*

simulations of the device application by evaluating the cytotoxicity deriving from contact or release of toxic compounds or the damage deriving from friction and rubbing with the tissue. In this sense, to challenge the performance of our model, we selected a clinically approved catheter generally inserted in blood vessels. Biological effect exerted was assessed by *direct contact*, placing the catheter in the lumen of the artificial vessel and no cytotoxic effect occurred from the contact of the medical device with bioprinted cells. Such test cannot be achieved using 2D cell culture and normally requires an assessment with *in vivo* implantation in animal models. Thus, the biomimetic complexity achieved with this biofabrication process offers the opportunity to develop innovative testing methods that yield more precise and comprehensive biocompatibility evaluations, in accordance with the 3Rs principle [20,50].

To permit the vessel perfusion, enhancing the biomimicry of our platform, a novel bioreactor was developed, called CuBiBox. This biocompatible device effectively isolates the culture chamber from the external environment while still allowing gas exchange. It also securely holds the vessel and facilitates the shipment. CuBiBox enables to investigate the impact of a solutions of interest flowing into the lumen, opening up exciting opportunities for conducting studies on cytotoxicity, drug delivery and adsorption, through specific mechanic or fluid dynamic conditions.

Furthermore, the CuBiBox bioreactor offers the future opportunity to adapt the vessel model for *in vitro* hemocompatibility investigations, where human blood passes into the artificial vessel coupled to other medical devices such as stents, cardiovascular implants and cutting-edge sensor devices. These findings could additionally serve as a blueprint for *in vitro* evaluation of hemolysis, thrombosis, the development of pseudointima or neointima, the simulation of various cardiovascular diseases and to perform specific assays that were previously only achievable through the animal experimentation.

## 5. Conclusions

In this study, we developed a new biofabrication approach combining bioprinting and FDG, to realize an artificial blood vessel that closely resembles its human counterpart in terms of cell composition and localization. This approach is feasible, versatile and the use of FDG helps to realize a thin internal layer, promoting endothelial cell migration and self-organization. The BBV has been employed to assess the toxicological effects of a biomedical device evaluating the *direct* and *indirect contact* cytotoxicity in a more comprehensive and reliable way than traditional 2D cell cultures, and without the need for animal models. Thanks to the realization of a customized bioreactor, the BBV can be perfused opening

unexplored possibilities for testing intravascular medical devices and studying human cardiovascular disease *in vitro*.

### Disclosure statement

No potential conflict of interest was reported by the author(s).

### Funding

The work was financially supported by the grants POR FESR 2014-2020 [ID: CUBIBOX] and by 'Progetto Dipartimenti Eccellenti MIUR 2017 and 2022'. The authors acknowledge B. Braun Avitum Italy for the supply of the catheter and Goldoni e Dondi srl for the support in design and realization of the CuBiBox bioreactor.

### Author contributions

Conceptualization: AP, EV, GM, LA; Row data acquisition: AP, VB, FG, GM; Data analysis: TP, ER, LR; Figure preparation: AP, AF; Writing original draft: AP, TP, SS; Validation: AF, LR, LA; Review and Editing: EV, MD; Founding: MD, SS.

### Ethical approval

This study does not contain any studies with human or animal subjects performed by any of the authors.

### References

- [1] International standard organization ISO 10993-1: 2021. Biological evaluation of medical devices - part 1: evaluation and testing within a risk management process. Available from: <https://www.iso.org/standard/68936.html>
- [2] FDA-2013-D-0350, International standard organization ISO 10993-1: 2021. Biological evaluation of medical devices - part 1: evaluation and testing within a risk management process. US Food Drug Adm. Available from: <https://www.fda.gov/regulatory-information/search-fda-guidance-documents/use-international-standard-iso-10993-1-biological-evaluation-medical-devices-part-1-evaluation-and>
- [3] Griffith LG, Swartz MA. Capturing complex 3D tissue physiology in vitro. *Nat Rev Mol Cell Biol.* 2006;7(3):211–224. doi: 10.1038/nrm1858
- [4] Pampaloni F, Reynaud EG, Stelzer EH. The third dimension bridges the gap between cell culture and live tissue. *Nat Rev Mol Cell Biol.* 2007;8(10):839–845. doi: 10.1038/nrm2236
- [5] Timm DM, Chen J, Sing D, et al. A high-throughput three-dimensional cell migration assay for toxicity screening with mobile device-based macroscopic image analysis. *Sci Rep.* 2013;3(1):3000. doi: 10.1038/srep03000
- [6] Petrachi T, Portone A, Arnaud GF, et al. Novel bio-printed 3D model to human fibrosis investigation. *Biomed Pharmacother.* 2023;165:115146. doi: 10.1016/j.biopha.2023.115146

- [7] Di Cesare M, Perel P, Taylor S, et al. The heart of the world. *Glob Heart.* 2024;19(1):11. doi: 10.5334/gh.1288
- [8] Xu L, Varkey M, Jorgensen A, et al. Bioprinting small diameter blood vessel constructs with an endothelial and smooth muscle cell bilayer in a single step. *Biofabrication.* 2020;12(4):045012. doi: 10.1088/1758-5090/aba2b6
- [9] Gao Q, Liu Z, Lin Z, et al. 3D bioprinting of vessel-like structures with multilevel fluidic channels. *ACS Biomater Sci Eng.* 2017;3(3):399–408. doi: 10.1021/acsbomaterials.6b00643
- [10] Jia L, Han F, Yang H, et al. Microfluidic fabrication of biomimetic helical hydrogel microfibers for blood-vessel-on-a-chip applications. *Adv Healthc Mater.* 2019;8(13):1900435. doi: 10.1002/adhm.201900435
- [11] Assmann A, Delfs C, Munakata H, et al. Acceleration of autologous in vivo recellularization of decellularized aortic conduits by fibronectin surface coating. *Biomaterials.* 2013;34(25):6015–6026. doi: 10.1016/j.biomaterials.2013.04.037
- [12] Syedain ZH, Meier LA, Bjork JW, et al. Implantable arterial grafts from human fibroblasts and fibrin using a multi-graft pulsed flow-stretch bioreactor with noninvasive strength monitoring. *Biomaterials.* 2011;32(3):714–722. doi: 10.1016/j.biomaterials.2010.09.019
- [13] O'Connor C, Brady E, Zheng Y, et al. Engineering the multiscale complexity of vascular networks. *Nat Rev Mater.* 2022;7(9):702–716. doi: 10.1038/s41578-022-00447-8
- [14] Fazal F, Raghav S, Callanan A, et al. Recent advancements in the bioprinting of vascular grafts. *Biofabrication.* 2021;13(3):032003. doi: 10.1088/1758-5090/ac0963
- [15] Tavafoghi M, Darabi MA, Mahmoodi M, et al. Multimaterial bioprinting and combination of processing techniques towards the fabrication of biomimetic tissues and organs. *Biofabrication.* 2021;13(4):042002. doi: 10.1088/1758-5090/ac0b9a
- [16] Mota C, Camarero-Espinosa S, Baker MB, et al. Bioprinting: from tissue and organ development to in vitro models. *Chem Rev.* 2020;120(19):10547–10607. doi: 10.1021/acs.chemrev.9b00789
- [17] Peng W, Unutmaz D, Ozbolat IT. Bioprinting towards physiologically relevant tissue models for pharmaceuticals. *Trends Biotechnol.* 2016;34(9):722–732. doi: 10.1016/j.tibtech.2016.05.013
- [18] Nie J, Gao Q, Fu J, et al. Grafting of 3D bioprinting to in vitro drug screening: a review. *Adv Healthc Mater.* 2020;9(7):1901773. doi: 10.1002/adhm.201901773
- [19] Jain P, Kathuria H, Dubey N. Advances in 3D bioprinting of tissues/organs for regenerative medicine and in-vitro models. *Biomaterials.* 2022;287:121639. doi: 10.1016/j.biomaterials.2022.121639
- [20] Stengel E, Thiele J, Seiffert S. Multiparametric material functionality of microtissue-based in vitro models as alternatives to animal testing. *Adv Sci.* 2022;9(10):2105319. doi: 10.1002/advs.202105319
- [21] Gao G, Kim BS, Jang J, et al. Recent strategies in extrusion-based three-dimensional cell printing toward organ biofabrication. *ACS Biomater Sci Eng.* 2019;5(3):1150–1169. doi: 10.1021/acsbomaterials.8b00691
- [22] Krishnamoorthy S, Zhang Z, Xu C. Biofabrication of three-dimensional cellular structures based on gelatin

- methacrylate–alginate interpenetrating network hydrogel. *J Biomater Appl.* **2019**;33(8):1105–1117. doi: [10.1177/0885328218823329](https://doi.org/10.1177/0885328218823329)
- [23] Xu C, Chai W, Huang Y, et al. Scaffold-free inkjet printing of three-dimensional zigzag cellular tubes. *Biotechnol Bioeng.* **2012**;109(12):3152–3160. doi: [10.1002/bit.24591](https://doi.org/10.1002/bit.24591)
- [24] Christensen K, Xu C, Chai W, et al. Freeform inkjet printing of cellular structures with bifurcations. *Biotechnol Bioeng.* **2015**;112(5):1047–1055. doi: [10.1002/bit.25501](https://doi.org/10.1002/bit.25501)
- [25] Liu Y, Zhang Y, Jiang W, et al. A novel biodegradable multilayered bioengineered vascular construct with a curved structure and multi-branches. *Micromachines.* **2019**;10(4):275. doi: [10.3390/mi10040275](https://doi.org/10.3390/mi10040275)
- [26] Dobos A, Gantner F, Markovic M, et al. On-chip high-definition bioprinting of microvascular structures. *Biofabrication.* **2020**;13(1):015016. doi: [10.1088/1758-5090/abb063](https://doi.org/10.1088/1758-5090/abb063)
- [27] Gao G, Lee JH, Jang J, et al. Tissue engineered bio-blood-vessels constructed using a tissue-specific bioink and 3D coaxial cell printing technique: a novel therapy for ischemic disease. *Adv Funct Mater.* **2017**;27(33):1700798. doi: [10.1002/adfm.201700798](https://doi.org/10.1002/adfm.201700798)
- [28] Zhang YS, Haghiastiani G, Hübscher T, et al. 3D extrusion bioprinting. *Nat Rev Methods Primer.* **2021**;1(1):1–20. doi: [10.1038/s43586-021-00073-8](https://doi.org/10.1038/s43586-021-00073-8)
- [29] Bittner SM, Guo JL, Mikos AG. Spatiotemporal control of growth factors in three-dimensional printed scaffolds. *Bioprinting.* **2018**;12:e00032. doi: [10.1016/j.bprint.2018.e00032](https://doi.org/10.1016/j.bprint.2018.e00032)
- [30] Xu S, Li Q, Pan H, et al. Tubular silk fibroin/gelatin–tyramine hydrogel with controllable layer structure and its potential application for tissue engineering. *ACS Biomater Sci Eng.* **2020**;6(12):6896–6905. doi: [10.1021/acsbomaterials.0c01183](https://doi.org/10.1021/acsbomaterials.0c01183)
- [31] Ouyang L, Burdick JA, Sun W. Facile biofabrication of heterogeneous multilayer tubular hydrogels by fast diffusion-induced gelation. *ACS Appl Mater Interfaces.* **2018**;10(15):12424–12430. doi: [10.1021/acsami.7b19537](https://doi.org/10.1021/acsami.7b19537)
- [32] Mredha MTI, Jeong S-G, Seon J-K, et al. A diffusion-driven fabrication technique for anisotropic tubular hydrogels. *Soft Matter.* **2018**;14(37):7706–7713. doi: [10.1039/C8SM01235K](https://doi.org/10.1039/C8SM01235K)
- [33] Ma S, Rong M, Lin P, et al. Fabrication of 3D tubular hydrogel materials through on-site surface free radical polymerization. *Chem Mater.* **2018**;30(19):6756–6768. doi: [10.1021/acs.chemmater.8b02532](https://doi.org/10.1021/acs.chemmater.8b02532)
- [34] International standard organization ISO 10993-5: 2009. Biological evaluation of medical devices - part 5: tests for in vitro cytotoxicity. Available from: <https://www.iso.org/standard/36406.html>
- [35] International standard organization ISO 10993-12: 2021. Biological evaluation of medical devices - part 12: sample preparation and reference materials. Available from: <https://www.iso.org/standard/75769.html>
- [36] Candini O, Grisendi G, Foppiani EM, et al. A novel 3D in vitro platform for pre-clinical investigations in drug testing, gene therapy, and immuno-oncology. *Sci Rep.* **2019**;9(1):7154. doi: [10.1038/s41598-019-43613-9](https://doi.org/10.1038/s41598-019-43613-9)
- [37] Maestri CA, Bettotti P, Scarpa M. Fabrication of complex-shaped hydrogels by diffusion controlled gelation of nanocellulose crystallites. *J Mater Chem B.* **2017**;5(40):8096–8104. doi: [10.1039/C7TB01899A](https://doi.org/10.1039/C7TB01899A)
- [38] International standard organization ISO 10993-23: 2021. Biological evaluation of medical devices - part 23: tests for irritation. Available from: <https://www.iso.org/standard/74151.html>
- [39] Kawecki F, L’Heureux N. Current biofabrication methods for vascular tissue engineering and an introduction to biological textiles. *Biofabrication.* **2023**;15(2):022004. doi: [10.1088/1758-5090/acbf7a](https://doi.org/10.1088/1758-5090/acbf7a)
- [40] Neufeld L, Yeini E, Pozzi S, et al. 3D bioprinted cancer models: from basic biology to drug development. *Nat Rev Cancer.* **2022**;22(12):679–692. doi: [10.1038/s41568-022-00514-w](https://doi.org/10.1038/s41568-022-00514-w)
- [41] Miller JS, Stevens KR, Yang MT, et al. Rapid casting of patterned vascular networks for perfusable engineered three-dimensional tissues. *Nat Mater.* **2012**;11(9):768–774. doi: [10.1038/nmat3357](https://doi.org/10.1038/nmat3357)
- [42] Kutty JK, Cho E, Soo Lee J, et al. The effect of hyaluronic acid incorporation on fibroblast spreading and proliferation within peg-diacrylate based semi-interpenetrating networks. *Biomaterials.* **2007**;28(33):4928–4938. doi: [10.1016/j.biomaterials.2007.08.007](https://doi.org/10.1016/j.biomaterials.2007.08.007)
- [43] Jain M, He Q, Lee WS, et al. Role of CD44 in the reaction of vascular smooth muscle cells to arterial wall injury. *J Clin Invest.* **1996**;97(3):596–603. doi: [10.1172/JCI118455](https://doi.org/10.1172/JCI118455)
- [44] Lokeshwar VB, Iida N, Bourguignon LYW. The cell adhesion molecule, GP116, is a new CD44 variant (ex14/v10) involved in hyaluronic acid binding and endothelial cell proliferation \*. *J Biol Chem.* **1996**;271(39):23853–23864. doi: [10.1074/jbc.271.39.23853](https://doi.org/10.1074/jbc.271.39.23853)
- [45] Mandal BB, Kundu SC. Cell proliferation and migration in silk fibroin 3D scaffolds. *Biomaterials.* **2009**;30(15):2956–2965. doi: [10.1016/j.biomaterials.2009.02.006](https://doi.org/10.1016/j.biomaterials.2009.02.006)
- [46] Bertassoni LE, Cardoso JC, Manoharan V, et al. Direct-write bioprinting of cell-laden methacrylated gelatin hydrogels. *Biofabrication.* **2014**;6(2):024105. doi: [10.1088/1758-5082/6/2/024105](https://doi.org/10.1088/1758-5082/6/2/024105)
- [47] Wang H, Zhou L, Liao J, et al. Cell-laden photocrosslinked GelMA–DexMA copolymer hydrogels with tunable mechanical properties for tissue engineering. *J Mater Sci Mater Med.* **2014**;25(9):2173–2183. doi: [10.1007/s10856-014-5261-x](https://doi.org/10.1007/s10856-014-5261-x)
- [48] Shie M-Y, Lee J-J, Ho C-C, et al. Effects of gelatin methacrylate bio-ink concentration on mechano-physical properties and human dermal fibroblast behavior. *Polymers.* **2020**;12(9):1930. doi: [10.3390/polym12091930](https://doi.org/10.3390/polym12091930)
- [49] Martinez-Garcia FD, Valk MM, Sharma PK, et al. Adipose tissue-derived stromal cells alter the mechanical stability and viscoelastic properties of gelatine methacryloyl hydrogels. *Int J Mol Sci.* **2021**;22(18):10153. doi: [10.3390/ijms221810153](https://doi.org/10.3390/ijms221810153)
- [50] Maestri E. The 3Rs principle in animal experimentation: a legal review of the state of the art in Europe and the case in Italy. *BioTech.* **2021**;10(2):9. doi: [10.3390/biotech1002009](https://doi.org/10.3390/biotech1002009)